Am J Physiol Heart Circ Physiol 305: H295–H304, 2013.
First published May 24, 2013; doi:10.1152/ajpheart.00990.2012.

CALL FOR PAPERS | *Mitochondria in Cardiovascular Physiology and Disease*

Glucagon-like peptide-1 receptor activation reverses cardiac remodeling via normalizing cardiac steatosis and oxidative stress in type 2 diabetes

Akio Monji,* Toko Mitsui,* Yasuko K. Bando, Morihiko Aoyama, Toshimasa Shigeta, and Toyoaki Murohara

Department of Cardiology, Nagoya University Graduate School of Medicine, Nagoya, Japan

Submitted 31 December 2012; accepted in final form 15 May 2013

Monji A, Mitsui T, Bando YK, Aoyama M, Shigeta T, Murohara T. Glucagon-like peptide-1 receptor activation reverses cardiac remodeling via normalizing cardiac steatosis and oxidative stress in type 2 diabetes. *Am J Physiol Heart Circ Physiol* 305: H295–H304, 2013. First published May 24, 2013; doi:10.1152/ajpheart.00990.2012.—Glucagon-like peptide-1 receptor (GLP-1R) agonist exendin-4 (Ex-4) is a remedy for type 2 diabetes mellitus (T2DM). Ex-4 ameliorates cardiac dysfunction induced by myocardial infarction in preclinical and clinical settings. However, it remains unclear whether Ex-4 may modulate diabetic cardiomyopathy. We tested the impact of Ex-4 on two types of diabetic cardiomyopathy models, genetic (KK) and acquired T2DM induced by high-fat diet [diet-induced obesity (DIO)], to clarify whether Ex-4 may combat independently of etiology. Each type of mice was divided into Ex-4 (24 nmol·kg^{-1}·day^{-1} for 40 days; KK-ex4 and DIO-ex4) and vehicle (KK-v and DIO-v) groups. Ex-4 ameliorated systemic and cardiac insulin resistance and dyslipidemia in both T2DM models. T2DM mice exhibited systolic (DIO-v) and diastolic (DIO-v and KK-v) left ventricular dysfunctions, which were restored by Ex-4 with reduction in left ventricular hypertrophy. DIO-v and KK-v exhibited increased myocardial fibrosis and steatosis (lipid accumulation), in which were observed cardiac mitochondrial remodeling and enhanced mitochondrial oxidative damage. Ex-4 treatment reversed these cardiac remodeling and oxidative stress. Cytokine array revealed that Ex-4-sensitive inflammatory cytokines were ICAM-1 and macrophage colony-stimulating factor. Ex-4 ameliorated myocardial oxidative stress via suppression of NADPH oxidase 4 with concomitant elevation of antioxidants (SOD-1 and glutathione peroxidase). In conclusion, GLP-1R agonism reverses cardiac remodeling and dysfunction observed in T2DM via normalizing imbalance of lipid metabolism and related inflammation/oxidative stress.

diabetes mellitus; mitochondria; oxidative stress; glucagon-like peptide-1; insulin resistance

GLUCAGON-LIKE PEPTIDE-1 RECEPTOR (GLP-1R) agonist is one of the remedies for type 2 diabetes mellitus (T2DM) used for patients at an advanced stage in which refractory cases to oral hypoglycemic reagents (4). In addition to its therapeutic action on diabetic condition, accumulating evidence demonstrated that GLP-1R agonism ameliorates systolic dysfunction in preclinical (2, 22) and clinical heart failure after ischemic heart disease (3, 20). Furthermore, recent reports have demonstrated the GLP-1 analog liraglutide ameliorates liver (19) and cardiac steatosis via modulation on the endoplasmic reticulum (ER) stress (24) in diet-induced obesity (DIO) mice. However, to our knowledge, it remains unclear whether the GLP-1R agonism may ameliorate cardiac remodeling and dysfunction observed in T2DM.

Suggested cardiac remodeling observed in overnutrition, such as obesity and T2DM, is illustrated by the histologic characteristics, i.e., cardiac fibrosis, myocardial hypertrophy, and steatosis of myocardium (29), at least in part, because of lipotoxity to heart (36). The presence of overnutrition results in alterations in not only systemic but also cardiac insulin resistance (6), fatty acid transport/storage/oxidation, oxygen consumption, and redox status, leading to the mitochondrial damages and subsequent maladaptive cardiac remodeling and dysfunction (5, 6, 36); however, it remains unclear whether systemic intervention by GLP-1R agonism for the overnutrition state may concomitantly reverse the relevant cardiac remodeling and dysfunction.

Accordingly, we hypothesized whether the GLP-1R activator exendin-4 (Ex-4) may mitigate cardiac dysfunction and remodeling occurred in T2DM by ameliorating cardiac oxidative stress that was presumably induced by concomitant steatosis and/or enhanced insulin resistance. To elucidate this notion more universally, we tested the impact of Ex-4 on diabetic heart by used of 2 distinct T2DM models, genetic and acquired T2DM induced by high-fat diet (HFD; DIO).

METHODS

Mice models. All procedures involving mice were approved by the Institutional Animal Care and Use Committee of Nagoya University. Two types of T2DM models were allocated: genetic T2DM model (KKAy) (14, 35) and age- and sex-matched (male)-acquired T2DM mice fed with high-fat diet (HFD60, Oriental Yeast, Tokyo, Japan) (32). Mice were allocated into experimental groups as follows: Ex-4 (24 nmol·kg^{-1}·day^{-1}, subcutaneously administrated by osmotic pump for 40 days; KK-ex4 and DIO-ex4; Sigma-Aldrich) and vehicle groups (KK-v and DIO-v). The overview of experimental protocol regarding mice feeding and drug treatment that applied to the present study was displayed in Fig. 1. The food consumption was measured by weighing new and remaining food three times weekly according to the previous report (19). Changes in food intake of individual mouse was expressed as the average value of food intake that was calculated from daily food intake for the whole experimental course. Oral glucose tolerance test was performed as follows: mice were subjected 6 h fasting, and glucose (2 g/kg body wt) was orally administered. Changes in blood glucose level were measured using the handy glucometer system (Sanwa-Kagaku, Nagoya, Japan) at the time point of 0, 30, 60, and 120 min after the glucose loading.

Blood chemistry. Blood glucose level was measured through a tail nick using a handheld glucometer. Plasma cholesterol and triglyceride

* A. Monji and T. Mitsui equally contributed to this work.

Address for reprint requests and other correspondence: Y. K. Bando, Dept. of Cardiology, Nagoya Univ. Graduate School of Medicine, 65 Tsurumai-cho, Showa-ku, Nagoya, Aichi, 466-8550, Japan (e-mail: ybando@med.nagoya-u.ac.jp).

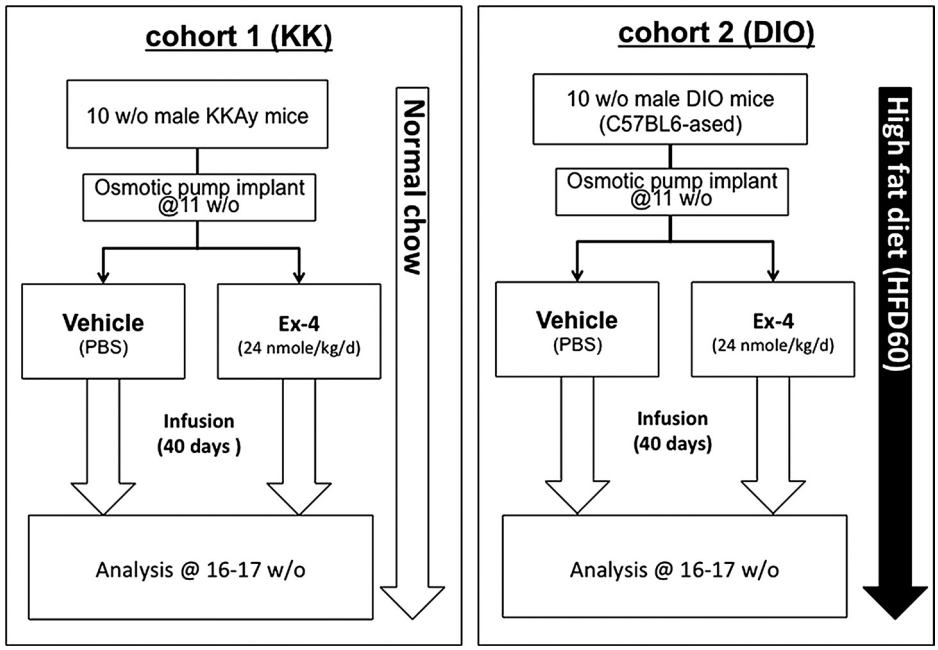

Fig. 1. Experimental protocol. Two cohorts of diabetic mouse models were allocated in the present study. *Cohort 1*, genetic type 2 diabetic model using KKAy (KK) mice; *cohort 2*, acquired type 2 diabetic mice induced by diet-induced obesity (DIO) mice of C57BL6 background. *Cohort 1* was fed with normal chow diet, and *cohort 2* was continuously fed with high-fat diet (60% fat content) to avoid diet-induced decline in body weight. w/o, without; d, day.

levels were measured using each blood specimen collected at the time of euthanizing from heart puncture of each mouse. Plasma insulin levels were determined by radioimmunoassay (Mouse Insulin RIA Kit; Millipore, MA).

Echocardiography. Cardiac function of each mouse was assessed using a complete two-dimensional and M-mode and Doppler echocardiogram [ACUSON Sequoia 512 system with a 15-MHz high-frequency transducer (Microson 15L8), Siemens]. Mice were anesthetized using a combination of ketamine (75 mg/kg) and xylazine (10 mg/kg) anesthesia to avoid any influence of the type of anesthesia on heart rate or left ventricular (LV) function (33).

Immunoblotting. Each heart tissue sample was subjected to frost shattering using Cryopress (Microtech Nichion, Chiba, Japan). Proteins were extracted in radioimmunoprecipitation assay buffer containing protease and phosphatase inhibitor cocktails. Equal amounts (10 μg) of protein from each group were electrophoresed and subjected to immunoblotting. Protein bands were detected using the following specific antibodies: phospho-insulin receptor substrate 1 (IRS-1) (Millipore), phospho-cAMP response element binding protein (CREB), GAPDH (Cell Signaling Technology), SOD-1 (Santa Cruz), and NADPH oxidases 4 (Nox4) and 2 (Nox2), glutathione peroxidase (GPx), and thioredoxin (TRx) (Abcam). The density of each protein band was analyzed using an image analysis software (ImageJ).

Cytokine array. A proteome profiler array was performed according to the manufacturer's instructions [Mouse Cytokine Array, Panel A (ARY006); R&D system, Minneapolis, MN]. In brief, after a 1-h membrane-blocking step, the preincubated mouse plasma-biotinylated antibody mixture was added, and the membrane was incubated overnight. After a series of washes, the membrane was incubated with horseradish peroxidase-conjugated streptavidin, and the signal was detected by using X-ray film. Average protein expression levels were measured by densitometry (ImageJ).

Immunohistochemistry and microscopic analysis. Frozen sections of heart tissue (8 μm) were subjected to immunohistochemistry and examined under a fluorescence microscope (Axio Observer Z1, Carl Zeiss MicroImaging). The cell surface area and ceramide accumulation in cardiomyocytes were detected using the following specific antibodies: dystrophin (Novocastra) and ceramide (Sigma), respectively. Each result was quantified by use of the ImageJ software as described previously (33).

Cardiac cAMP concentration. Frost-shattered heart samples using the Cryopress were subjected to cAMP concentration measurement using commercially available kit according to the manufacturer's protocols (Promega, WI).

Cardiac superoxide detection. For detection of cardiac superoxide radical levels, we used specific fluorescence dye dihydrothidium (DHE) as a probe (Invitrogen Molecular Probes). The sources of reactive oxygen species (ROS), including superoxide, are derived from mitochondrial respiratory chain and nonrespiratory chain origins (5, 28). To dissect out the source of ROS originated from mitochondrial respiratory chain, each heart section was pretreated with rotenone (100 μM), the inhibitor for mitochondrial electron chain complex I, and subjected to DHE staining (1 μM). To detect the mitochondria-specific oxidative stress level, each heart section was loaded

Table 1. *Effects of exendin-4 on body weight, heart weight, and glucose metabolism*

	KK-v	KK-ex4	DIO-v	DIO-ex4	CTL-v
BW, g	54 ± 1	52 ± 2	44 ± 1	35 ± 1	29 ± 1
HW, mg	223 ± 7	204 ± 8	140 ± 8	115 ± 1	136 ± 2
HW/BW	4.2 ± 0.2	3.7 ± 0.1	3.3 ± 0.1	3.3 ± 0.1	4.8 ± 0.1
BS, mg/dl	452 ± 114	468 ± 82	159 ± 14	143 ± 6	154 ± 23
Ins, μg/l	5.9 ± 0.5	2.9 ± 0.4*	3.1 ± 0.3	1.7 ± 0.4**	1.6 ± 0.3

Values are means ± SE; n = 3-10 for congenital type 2 diabetes mellitus mice (KK), and n = 3-9 for diet-induced obese mice. KK and DIO mice with vehicle treatment (KK-v and DIO-v, respectively) and the exendin-4 treated KK and DIO mice (KK-ex4 and DIO-ex4, respectively) and lean control mice (CTL) are shown. BW, body weight; BS, nonfasting blood sugar concentration; Ins, nonfasting plasma insulin concentration. $^{**}P < 0.01$ and $^{*}P < 0.05$ ves. vehicle counterpart.

with mitochondrial fluorescence probes mirotracker red (100 nM MTR; CM-H2XRos) in the presence of 200 nM mitotracker green, which is a carbocyanine-based mitochondrion-specific probe and detects all mitochondria by covalently binding to the inner mitochondrial membrane independently of membrane potential. MTR is nonfluorescent at baseline, and it becomes fluorescent once MTR is oxidized by ROS within mitochondria.

Transmission electron microscopy. Small pieces of LV myocardium were obtained from the LV free wall of adult male mice; fixed in Karnovsky's solution consisting of 2% paraformaldehyde, 2.5% glutaraldehyde, and 0.1 M phosphate buffer; and processed until embedding into epon plastic. Ultrathin sections were stained with 1% (wt/vol) uranyl acetate followed by Reynold's lead citrate. Micrographs were collected using a JEM-1400 transmission electron microscope (JEOL, Tokyo, Japan) at 100 kV and lower (×1,000) and higher (×5,000 and ×8,000) magnification. Scanned micrographs were analyzed using ImageJ software for the calculation of mitochondrial area and total mitochondrial number.

Mitochondrial fractionation. Frost-shattered heart samples using the Cryopress were subjected to mitochondrial fractionation using

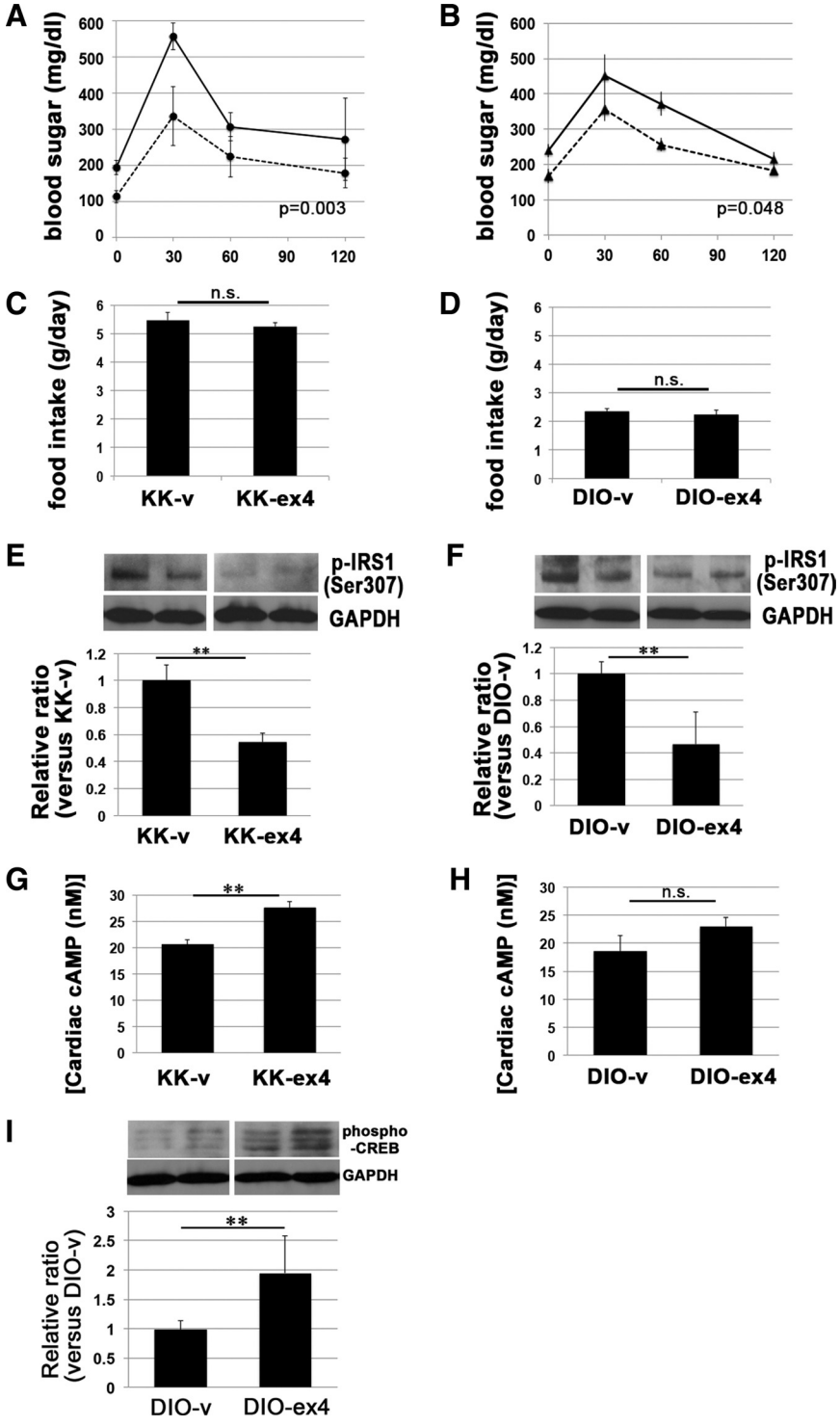

Fig. 2. Exendin-4 (Ex-4) ameliorated systemic and myocardial insulin resistance without affecting food intake. *A* and *B*: effect of Ex-4 treatment on impaired glucose tolerance in KKAy (*A*) and DIO (*B*) mice. Mice were subjected 6 h fasting, and glucose (2 g/kg body wt) was orally administered. Changes in blood glucose level were measured at the time point of 0, 30, 60, and 120 min after the glucose loading. Ex-4 ameliorated glucose tolerance both of KKAy ($P = 0.003$ by ANOVA) and DIO ($P = 0.048$ by ANOVA). *C* and *D*: mean of daily food intake of each mouse remain unchanged by administration of Ex-4. *E* and *F*: changes in cardiac insulin sensitivity were assessed by the phosphorylation level of insulin receptor substrate 1 (IRS-1). Increased IRS-1 phosphorylation levels indicates the impaired insulin sensitivity. *Left*: cardiac IRS-1 phosphorylation level of KKAy mice treated with vehicle (KK-v) and with Ex-4 (KK-ex4). *Right*: DIO with vehicle (DIO-v) and Ex-4 (DIO-ex4). Each panel of representative blot represents the results of 2 independent specimens obtained from the same group. GAPDH, internal control. *G* and *H*: effect of Ex-4 on cardiac cAMP concentrations in KKAy mice. The cAMP levels (in nM) were measured using each heart extract. *I*: changes in protein kinase A activity exhibited by the phospho-cAMP response element binding protein (CREB) level in DIO mouse hearts. $^{**}P < 0.01$ vs. vehicle counterpart ($n = 7$–10 for KK; $n = 4$–9 for DIO). ns, not significant.

density gradient procedure with commercially available kit (Pierce, Thermofisher Scientific), and each fraction was subjected to immunoblot analysis using antibodies of anti-Parkin (Abcam), anti-PTEN-induced kinase 1 (PINK1) (MerckMillipore, MA), anti-voltage-dependent anion channel (Abcam), anti-mitofusin-1 (Mfn1) (Santa Cruz, CA), and anti-Mfn2 (Sigma).

Statistical analyses. Data are expressed as means ± SE. Data analyses were performed using commercially available JMP software (JMP, version 8.0, SAS Institute). For comparisons between two groups, we employed Student's *t*-tests and ANOVA as appropriate. Values of $P < 0.05$ were considered statistically significant.

RESULTS

Ex-4 ameliorated systemic and myocardial insulin resistance and cardiac function without affecting food intake. Previous reports demonstrated GLP-1 analog liraglutide mitigates glucose intolerance and reduced heart mass without affecting body weight in mice (19, 24). We first examined the effects of Ex-4 on glucose homeostasis and changes in body and heart weight of KK and DIO mice (Table. 1). Ex-4 treatment ameliorated hyperinsulinemia and heart weight both in KK and DIO groups, whereas it had no effect on each body weight or postprandial blood glucose levels (19). To evaluate the impact of Ex-4 on systemic glucose intolerance more precisely, we performed oral glucose tolerance test, demonstrating that the 40-day Ex-4 treatment significantly ameliorated glucose intolerance both in KK (Fig. 2*A*) and DIO (Fig. 2*B*) without affecting the extent of food intake of each group (Fig. 2, *C* and *D*).

Impaired cardiac insulin signaling elicits mitochondrial damage leading to oxidative stress in heart, leading to cardiac remodeling and dysfunction (6). To further examine the effect of Ex-4 treatment on cardiac insulin sensitivity, we next assessed changes in phosphorylation level of IRS-1 (1) (Fig. 2, *E* and *F*). As expected, the cardiac IRS-1 phosphorylation levels were decreased both in KK-ex4 (Fig. 2*E*) and DIO-ex4 (Fig. 2*F*), suggesting that Ex-4 treatment ameliorated cardiac insulin resistance in those T2DM mice. Lastly, to confirm whether the systemic administration of Ex-4 may successfully act on heart, we measured cardiac cAMP concentration in each mouse heart, because GLP-1R activation generally promotes increase in intracellular cAMP level (10). Cardiac cAMP level was elevated in KK-ex4 compared with KK-v (Fig. 2*G*). In DIO-ex4 heart, we found the same trend of cAMP elevation; however, there was no statistical significance (Fig. 2*H*). We additionally examined the changes in cardiac phospho-CREB level of DIO-ex4, which is one of the surrogates for protein kinase A activation, and found marked elevation of phospho-CREB in DIO-ex4 heart (Fig. 2*I*). We next examined the impact of Ex-4 on cardiac function (Table 2) of each mouse. Echocardiography revealed that DIO-v exhibited systolic and diastolic LV dysfunction, which were restored by Ex-4 treatment with reduction in LV wall thickening. In KK-v, their systolic function remained unchanged, whereas those diastolic LV function was impaired and exhibited LV hypertrophy, which are consistent with characteristics to diabetic heart (5). Ex-4 reversed these diastolic dysfunction and LV hypertrophy of KK heart.

Ex-4 ameliorated cardiac remodeling observed in T2DM independently from etiology. We next examined the effects of Ex-4 on the cardiac remodeling induced by T2DM in terms of morphological changes (Fig. 3). Consistently with the findings observed in echocardiography (Table 2), histological analysis revealed that T2DM increased cardiomyocyte size, which was reversed by Ex-4 treatment (Fig. 3, *A* and *B*). Diabetic heart exhibits enhanced cardiac fibrosis (33, 39). We thus evaluated changes in cardiac fibrosis by Sirius red staining (Fig. 3, *C* and *D*). In KK-v and DIO-v, the Sirius red-positive fibrotic area was markedly increased, which were suppressed both in KK-ex4 (Fig. 3*C*) and DIO-ex4 groups (Fig. 3*D*).

We next examined the effects of Ex-4 on the cardiac mitochondrial remodeling observed in T2DM by transition electron microscopy (Fig. 3, *E–H*). In KK-v (Fig. 3*E*, *top*) and DIO-v (Fig. 3*F*, *top*), most mitochondrial cristae structure were destroyed and defragmented, leading to reduction in size (Fig. 3*G*) and increase in number (Fig. 3*H*). Ex-4 ameliorated those morphological changes of mitochondria both in KK and DIO mice (Fig. 3, *E–H*, *bottom*).

Ex-4 ameliorated cardiac mitochondrial remodeling observed in T2DM presumably via reduction of oxidative stress. To further clarify the effects of Ex-4 on the morphological changes of cardiac mitochondria detected by transition electron microscopy, we next conducted several experiments for detecting mitochondrial damage more specifically (Fig. 4). Because we found that both KK and DIO heart exhibited cardiac insulin resistance, which was reported to promote mitochondrial dysfunction and oxidative stress in the heart (6), we next hypothesized whether Ex-4 may ameliorate mitochondrial remodeling in diabetic heart via reduction of mitochondrial oxidative stress

Table 2. *Effects of exendin-4 on cardiac function of diabetic models*

	KK-v	KK-ex4	DIO-v	DIO-ex4	CTL-v
IVSd, mm	1.2 ± 0.1	1.0 ± 0.1*	1.1 ± 0.1	0.8 ± 0.1*	0.8 ± 0.1
LVPWd, mm	1.1 ± 0.1	1.0 ± 0.1*	1.0 ± 0.1	0.8 ± 0.1*	0.8 ± 0.1
LVDd, mm	3.7 ± 0.1	3.6 ± 0.1	3.6 ± 0.1	3.3 ± 0.2*	3.5 ± 0.1
LVDs, mm	2.3 ± 0.1	2.3 ± 0.1	2.5 ± 0.1	2.1 ± 0.1*	2.2 ± 0.1
EF, %	73 ± 1	72 ± 1	65 ± 1	74 ± 1**	73 ± 2
FS, %	37 ± 1	35 ± 1	30 ± 1	37 ± 1**	38 ± 2
E, m/s	0.8 ± 0.1	0.9 ± 0.1*	1.0 ± 0.1	1.2 ± 0.1*	0.8 ± 0.1
A, m/s	0.5 ± 0.1	0.4 ± 0.1	0.6 ± 0.1	0.6 ± 0.1	0.3 ± 0.1
E/*A* ratio	2.3 ± 0.1	2.8 ± 0.2**	1.6 ± 0.1	2.2 ± 0.2**	2.7 ± 0.1
DcT, ms	45 ± 1	37 ± 1*	43 ± 1	36 ± 1*	32 ± 2

Values are means ± SE; $n = 7$ for KK, and $n = 9$ for DIO. Systolic and diastolic left-ventricular (LV) functions were evaluated by echocardiogram. IVSd, diastolic interventricular septal wall thickness; LVPWd, diastolic LV posterior wall thickness; LVDd, diastolic LV diameter; LVDs, systolic LV diameter; EF, LV ejection fraction; FS, LV fraction shortening; *E*, mitral Doppler-flow velocity E wave; *A*, mitral Doppler-flow velocity A wave; Dct, deceleration time of mitral early inflow. $^{**}P < 0.01$ and $^{*}P < 0.05$ vs. vehicle counterpart.

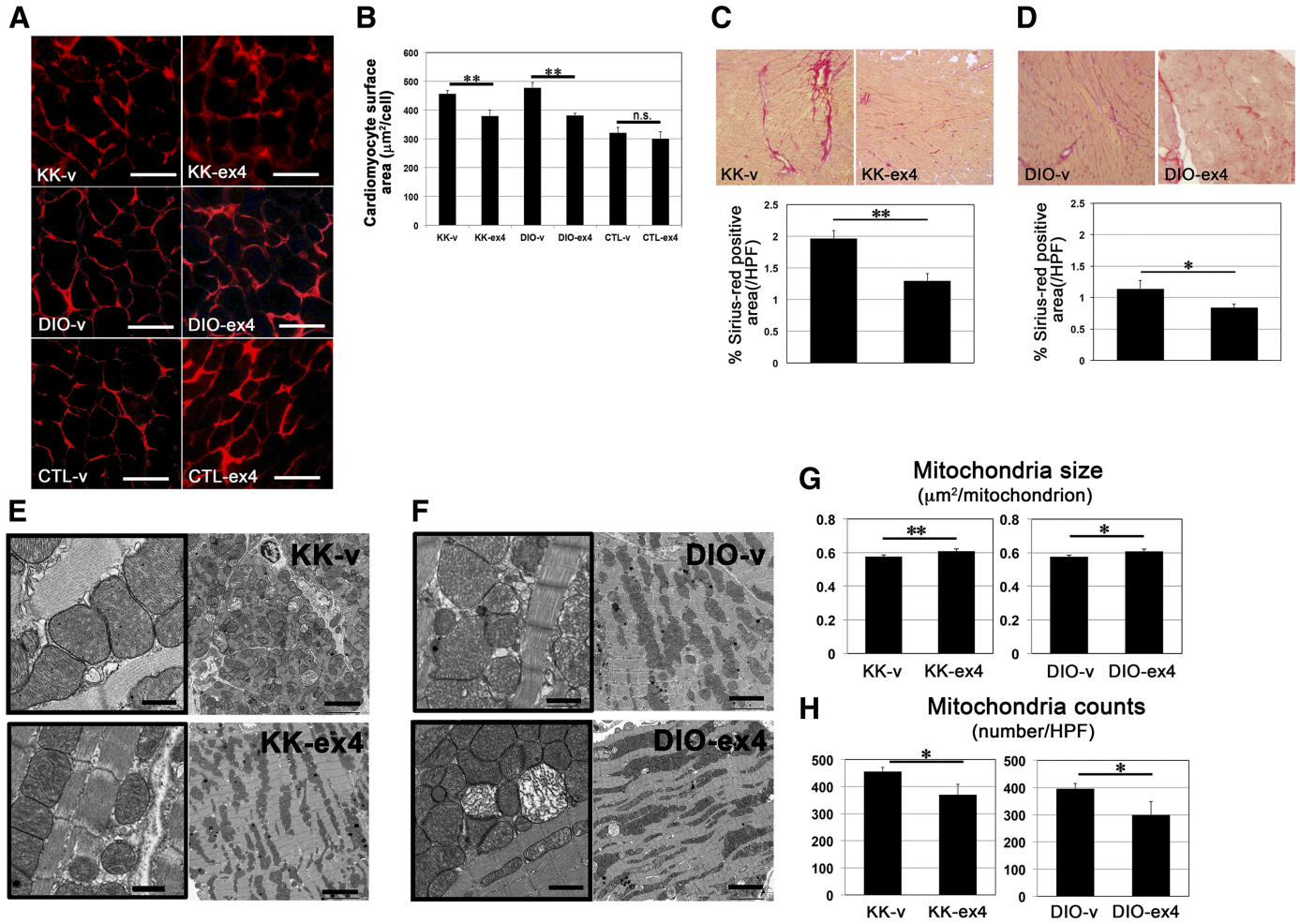

Fig. 3. Ex-4 reduced cardiomyocyte size and cardiac fibrosis and ameliorated mitochondrial remodeling in diabetic myocardium. Effects of Ex-4 on changes in cardiac remodeling assessed by histologic analysis. *A* and *B*: each cardiomyocyte surface area was detected by immunofluorescence using anti-dystrophin antibody (red, *A*). *Top*: heart sections obtained from KK-v (*left*) and KK-ex4 (*right*). *Middle*: DIO-v (*left*) and DIO-ex4 (*right*). *Bottom*: lean control (CTL-v, *right*) and lean mice treated with Ex-4 (CTL-ex4). *Bottom*: Ex-4-treated groups of KK (*left*), DIO (*middle*), and lean control (*right*). Data were summarized in bar graph. $^{**}P < 0.01$ vs. vehicle counterpart (n = 7–10). *C* and *D*: changes in cardiac fibrosis detected by Sirius-red staining. The Sirius-red-positive fibrotic area were measured by conversion of densitometric data and summarized in each graph represented below the representative images: KK-v and KK-ex4 (*C*), DIO-v and DIO-ex4 (*D*). $^{**}P < 0.01$ and $^{*}P < 0.05$ vs. vehicle counterpart (n = 7–10). *E–H*: effects of Ex-4 on mitochondrial remodeling observed in diabetic myocardium by transition electron microscopy (TEM). Each pair of TEM images displayed a set of higher magnification (*left*; scale bar, 1 μm) and those observed at a lower magnification (*right*; scale bar, 5 μm). *E*, *top*: KK-v heart. *E*, *bottom*: KK-ex4. *F*, *top*: DIO-v heart. *F*, *bottom*: DIO-ex4. *G* and *H*: summary of mitochondrial morphologic changes in TEM images. Bar graphs indicate mean mitochondria size (*G*) and counts (*H*) per lower magnification images. $^{*}P < 0.05$ (n = 4–6). HPF, high power field.

(Fig. 4, *A–C*). Mitotracker red (MTR), a useful indicator for mitochondria-specific oxidative stress level, revealed that the MTR-positive spots were markedly increased both of KK and DIO hearts compared with the nondiabetic counterpart (Fig. 4, *A–C*), which were diminished in Ex-4-treated mouse hearts [for KK (Fig. 4*A*, *left*) and DIO (Fig. 4*B*, *left*)].

Mfn1 and Mfn2 are mitochondrial regulatory proteins that determine mitochondria morphological changes and dynamics via regulating fission/fusion, and the endogenous levels of Mfn1 attenuate cardiomyocyte viability in the face of an imminent oxidative stress (ROS) observed in obesity (25). Using mitochondrial fractionation, we next examined changes in Mfn1 and Mfn2 levels as a probe for diabetes-mediated mitochondrial damage. Both of KK and DIO groups, their Mfn1/Mfn2 ratio was found to be reduced by Ex-4-treated groups (Fig. 4, *D* and *E*, *left*). We further confirmed the impact of Ex-4 on mitochondrial damage observed in T2DM heart by use of another surrogate for mitochondrial damage, PARKIN and PINK, of which complex accumulates specifically to the damaged mitochondria observed in a ROS-mediated mitophagy (12, 37). In KK-v (Fig. 4*F*) and DIO-v (Fig. 4*G*), both PARKIN and PINK1 levels were abundant in each mitochondrial fraction, which was reversed by Ex-4 treatment.

Ex-4 reduced cardiac lipid accumulation and inflammatory cytokines in T2DM. Obesity causes enhancing of not only oxidative stress but also local/systemic inflammation, which links obesity-related insulin resistance (13, 40). New evidence exploring the mechanisms linking ROS and inflammation find that ROS derived from mitochondria act as signal-transducing molecules that provoke the upregulation of inflammatory cytokines (21). Furthermore, ample evidence demonstrates that Ex-4 was reported to exert anti-inflammatory effects in human

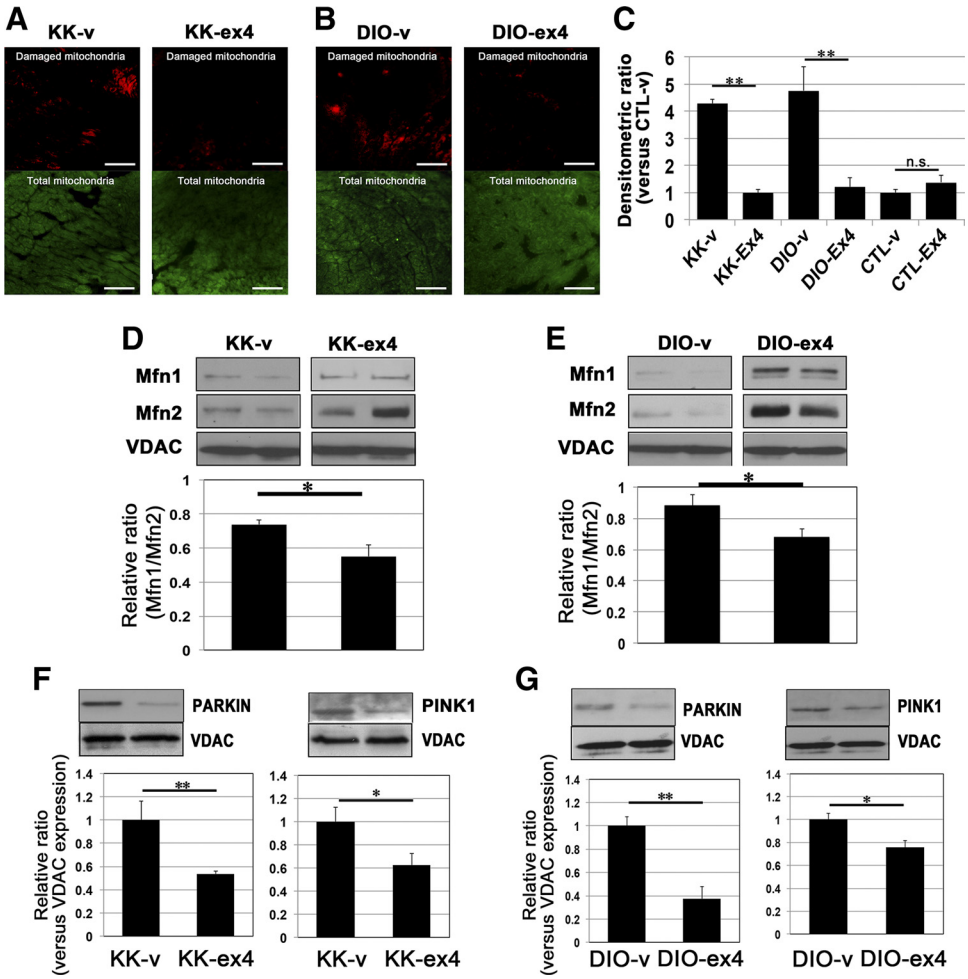

Fig. 4. Ex-4 ameliorated cardiac mitochondrial oxidative stress and damage in diabetic myocardium. *A* and *B*: mitochondria-specific oxidative stress was detected by mirotracker red (MTR, 100 nM) in the presence of mitotracker green (200 nM) as a control detecting total mitochondria. MTR becomes red once MTR is oxidized by reactive oxygen species within mitochondria: KK-v and KK-ex4 (*A*) and DIO-v and DIO-ex4 (*B*). Data were converted as densitometric ratio vs. CTL-v and summarized in bar graph (*C*). $^{**}P < 0.01$ and $^{*}P < 0.05$. *D–G*: protective effect of Ex-4 on mitochondrial damage. Changes in mitofusin 1 and 2 (Mfn1/2) ratio (*D* and *E*) and mitophagy modulator Parkin (PARKIN) and PTEN-induced kinase 1 (PINK) levels (*F* and *G*) were assessed using mitochondria fractionation of each heart extract. Densitometry data were summarized as the relative ratio vs. those voltage-dependent anion channel (VDAC) as an internal control of standard mitochondrial proteins. $^{**}P < 0.01$ and $^{*}P < 0.05$ vs. vehicle counterpart.

(7) and in apolipoprotien-E knockout mice (26), which was presumably mediated by its another effect on lipid metabolism (7, 26). We thus hypothesized whether the impact of Ex-4 on the pathological lipid profile in T2DM may play a key role in its protective effects on diabetic myocardial remodeling. To elucidate this notion, we next examined the effect of Ex-4 on systemic and local/cardiac accumulation of lipids. We measured changes in plasma cholesterol levels and found that Ex-4 treatment decreased both total cholesterol (Fig. 5*A*) and triglyceride (Fig. 5*B*) levels in KK and DIO groups. GLP-1R agonism reduces very low-density lipoprotein production and hepatic steatosis (26). We next hypothesized whether Ex-4 may reduce cardiac steatosis, thereby normalizing cardiomyocyte size that occurred in T2DM (Fig. 5, *C* and *D*). Changes in cardiac steatosis were detected by ceramide staining, revealing that we found higher lipid accumulation to the heart in KK-v group (Fig. 5, *C* and *D*, *right* and *middle*), which was reversed by Ex-4 treatment (Fig. 5, *C* and *D*, *left top* and *left middle*). We also evaluated local lipid accumulation by use of Oil-red-O staining, which was found to be less sensitive than the case observed in ceramide staining; however, the distribution pattern of lipid in each diabetic heart seemed patchy, not uniformly diffuse (Fig. 5, *E* and *F*). We next aimed to specify any inflammatory cytokine that may be sensitive to Ex-4 treatment by use of cytokine array (Fig. 5, *G* and *H*). Both in KK (Fig. 5*G*) and DIO (Fig. 5*H*), Ex-4 treatment markedly reduced ICAM-1 and macrophage colony-stimulating factor (M-CSF). Regarding TNF-α, one of the cytokines modulating insulin resistance (15), it remained unchanged; we further confirmed this trend by measuring the plasma TNF-α level of each mouse using ELISA (data not shown).

Effects of GLP-1 receptor activation on cardiac oxidative stress and mitochondrial damage. Lastly, we examined the impact of Ex-4 on cardiac oxidative stress using superoxide-specific fluorescence dye DHE that detects superoxide derived from not only mitochondrial respiratory chain but also non-respiratory chain origins (5, 28). The DHE staining revealed that Ex-4 treatment reduced cardiac oxidative stress both in KK (Fig. 6*A*) and DIO (Fig. 6*B*). We further evaluated the mechanism(s) underlying the Ex-4-mediated antioxidant effects in terms of oxidative regulators (Nox2 and Nox4, SOD-1, TRx, and GPx). We found that cardiac Nox4 level was downregulated by Ex-4 despite the Nox2 level that remained unchanged (Fig. 6, *C* and *D*) both in DIO and KK. Of note, all of the antioxidant proteins we evaluated were increased in DIO-ex4 (Fig. 6*D*); however, those counterparts of KK-ex4 remained unaffected (Fig. 6*C*).

DISCUSSION

To date, it is getting familiar that metabolic disorders due to overnutrition such as T2DM and obesity promote cardiac

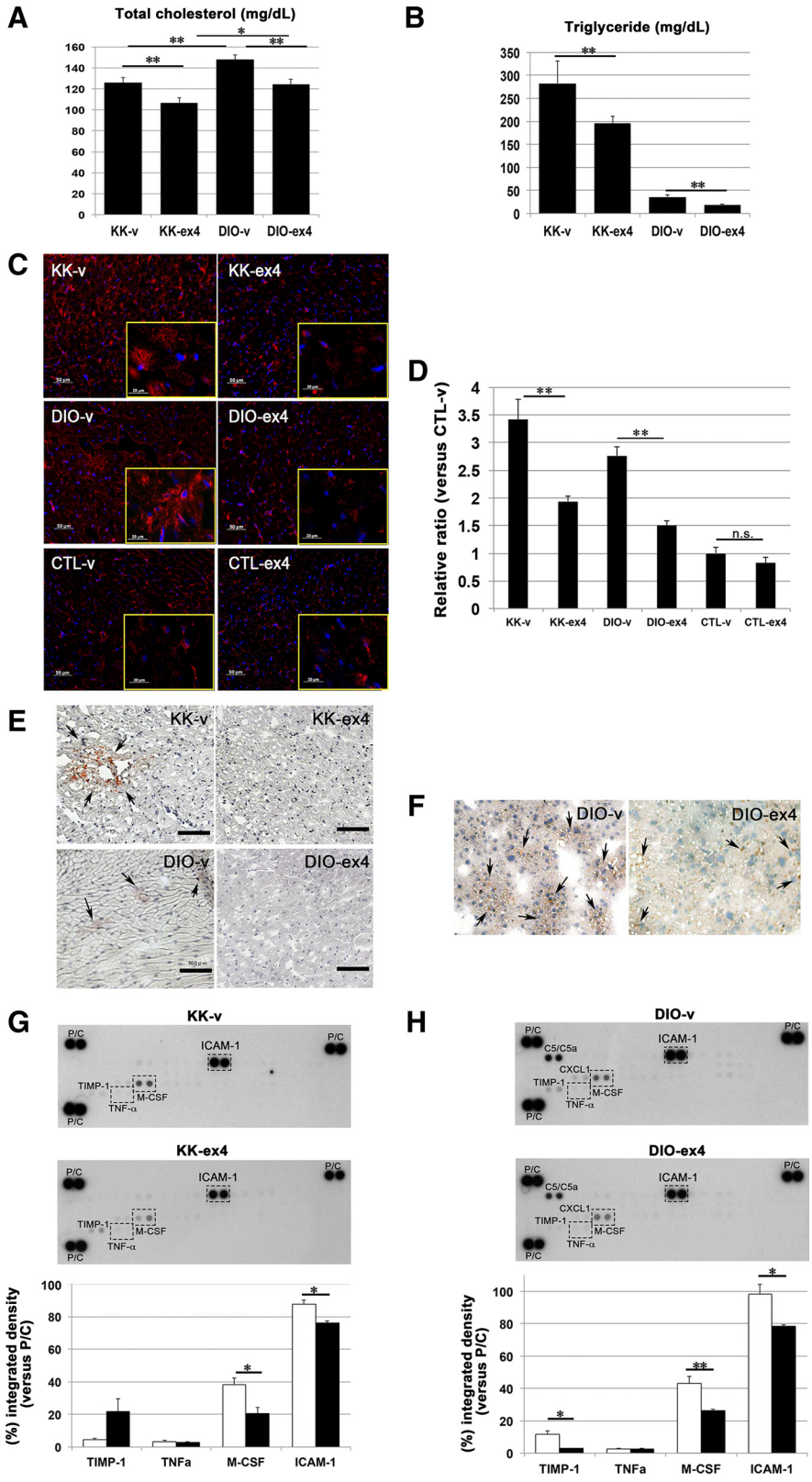

Fig. 5. Effect of Ex-4 on systemic and cardiac lipid levels and inflammatory cytokines. Effect of Ex-4 on plasma cholesterol (*A*) and triglyceride (*B*) levels. Ex-4 decreased both total cholesterol and triglyceride levels in KK and DIO groups. *C*: effect of Ex-4 on cardiac steatosis. Changes in cardiac steatosis were detected by ceramide staining (red). Both KK-v (*left*, *top*) and DIO-v (*left*, *middle*) exhibited higher lipid accumulation in the heart, which was reversed by Ex-4 treatment (*right*, *top* and *middle*). Scale bar = 50 μm (inset: 20 mm). Data were converted to densitometric value and summarized as a relative ratio vs. CTL-v (*D*). $^{**}P < 0.01$ vs. CTL-v (n = 7–10). *E* and *F*: lipid accumulation observed in myocardium (*E*) and liver (*F*). In myocardium, Oil-red-O staining revealed the lipid accumulation (arrow); however, its pattern was patchy and the number of positive spots was much less than the case observed in liver. Ex-4 reduced the Oil-red-positive spots both in myocardium and liver as previously reported. *G* and *H*: screening for Ex-4-sensitive inflammatory cytokine(s) using cytokine array. Representative blots obtained by specimen of KK (*G*) and DIO (*H*) were displayed. Data were summarized by densitometry (white bar, vehicle control; and black bar, Ex-4-treated group). Ex-4 partially but significantly reduced intercellular adhesion molecule-1 (ICAM-1) and macrophage colony-stimulating factor (M-CSF). Regarding tumor necrosis factor-α (TNF-α), it remained unchanged and likewise with other positively detected molecule: tissue inhibitor of metalloproteinase-1 (TIMP-1), complement 5/5a (C5/C5a), and chemokine (C-X-C motif) ligand 1 (CXCL1). P/C, positive control of each array. $^{**}P < 0.01$ and $^{*}P < 0.05$ vs. vehicle counterpart.

remodeling; however, it remains unclear whether therapeutic intervention for metabolic disorder may reverse these relevant cardiac remodeling. GLP-1, one of the incretine hormones, has been focused not only as an alternative therapeutic target for diabetes but also for its pleiotropic effects on cardiovascular disease, including heart failure related to pacing-induced heart failure (22), myocardial infarction (23), and obesity (24).

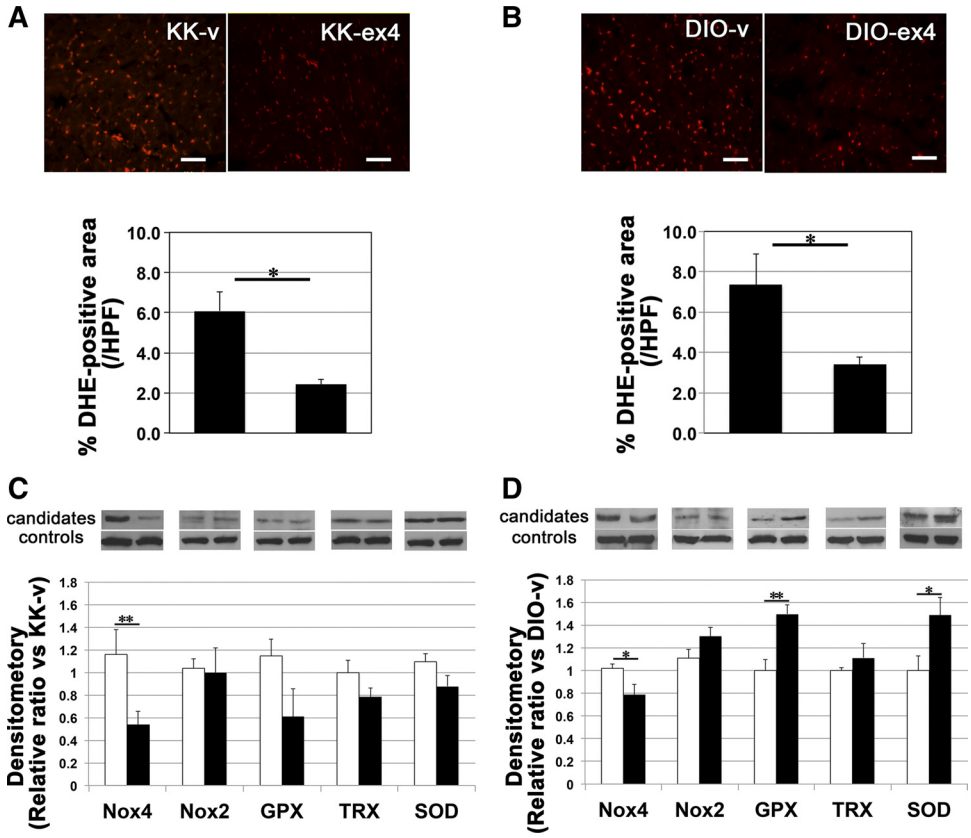

Fig. 6. Effect of Ex-4 treatment on cardiac oxidative stress. *A* and *B*: impact of Ex-4 on cardiac oxidative stress level detected by fluorescence dye dihydroethidium (DHE; red spots). Ex-4 reduced cardiac oxidative stress both in KK (*A*) and DIO (*B*). The DHE-positive area was quantified as a percentage in each total HPF (magnification, ×200) area. $*P < 0.05$ ($n = 7$–10). Scale bar = 50 μm. *C* and *D*: changes in oxidative stress-related molecules. Representative immunoblots displayed as a pair of reactive oxygen species-related molecules (candidates, *top*) as follows: NADPH oxidases (Nox: Nox2, Nox4), GPX glutathione peroxide (GPX), thioredoxine (TRX), and superoxide dismutase-1 (SOD). Each band was measured by densitometry and summarized in each graph represented below the representative images. White bar, vehicle-treated type 2 diabetes mellitus (T2DM) mice; black bar: Ex-4 treated. $**P < 0.01$; $*P < 0.05$ ($n = 7$–10).

Primary findings of the present study are as follows: *1*) GLP-1R agonist Ex-4 ameliorates cardiac remodeling and dysfunction observed in T2DM independently of etiology with concomitant amelioration of systemic and cardiac insulin resistance (Figs. 2–4); *2*) Ex-4 reduced circulating cholesterol levels (Fig. 5, *A* and *B*) and cardiac steatosis (Fig. 5, *C–E*); *3*) Ex-4 reduced circulating inflammatory cytokines, in particular, ICAM-1 and M-CSF (Fig. 5, *G* and *H*); *4*) Ex-4 reduced cardiac oxidative stress by reversing the levels of Nox-4 (KK and DIO) and antioxidant molecules (exclusively to DIO) (Fig. 6).

Recently, Noyan-Ashraf et al. (24) have reported the same trend regarding the impact of GLP-1-receptor analog on the obesity-induced cardiac dysfunction under distinct experimental conditions from those applied in the present study. Liraglutide, the protease-resistant analog of GLP-1, ameliorates cardiac dysfunction via improving cardiac inflammation and corresponding ER stress response, leading to improved cardiac dysfunction in animals on HFD by an AMP-activated protein kinase-dependent mechanism. They concluded that liraglutide had no effect on the of mitochondrial biogenesis and respiration by selected evaluation of those marker protein levels (PGC-1α, cytochrome *c*, and cytochrome-*c* oxidase subunit IV); however, their study did not demonstrate any change in mitochondrial remodeling as well as inflammatory cytokine/ROS target screening. Growing evidence demonstrates that ROS links to inflammation, and, in particular, mitochondria-derived ROS could provoke the upregulation of inflammatory cytokines (21), suggesting the underlying mechanisms of the GLP-1 axis-mediated amelioration of cardiac function could be explained at least two pathway by amelioration of cardiac mitochondrial remodeling by reducing cardiac ROS and inflammation as presented in the present study (Fig. 7) and by ER stress demonstrated by Noyan-Ashraf et al. (24).

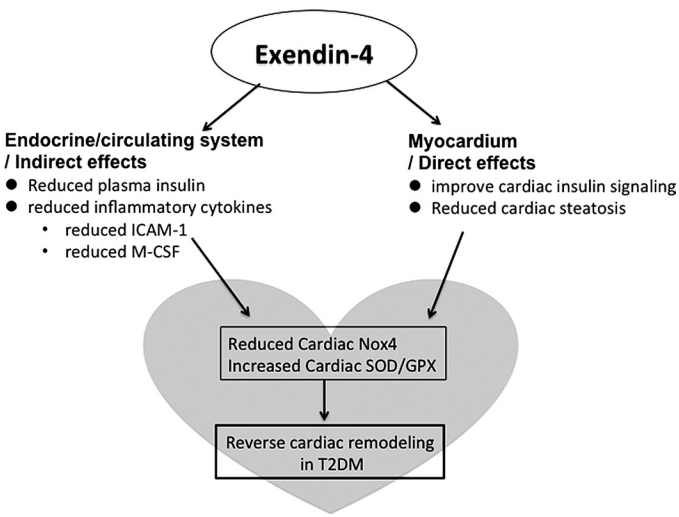

Fig. 7. Suggested mechanisms underlying the reversal effects of glucagon-like peptide-1 receptor activation on cardiac remodeling induced by type 2 diabetes. Overnutrition triggers dyslipidemia leading to abnormal lipid loading, which results in cardiac steatosis and insulin resistance presumably via inflammation and oxidative stress. Enhanced insulin resistance and lipotoxicity induced by cardiac steatosis promote enhanced oxidative stress that destroys mitochondrial integrity. Glucagon-like peptide-1 receptor activation counteracts these overnutrition-mediated dyslipidemia, cardiac steatosis, and cardiac insulin resistance.

We demonstrated that Ex-4 ameliorated systemic and cardiac insulin resistance (Fig. 2). Of note, cardiac insulin resistance links to ROS-mediated mitochondrial dysfunction (6). The Ex-4-mediated mitigation of impaired cardiac insulin signaling may also contribute to the reverse remodeling of diabetic myocardium. In addition, it is noteworthy that Nox-4 is presumably responsible for the Ex-4-mediated reduction of ROS (Fig. 6, *C* and *D*). It is noteworthy that Nox-4 is essential to insulin signal propagation (17) and cardiac remodeling (16, 18). Interestingly, Nox-4 signaling links to ICAM-1, which is an inflammatory mediator that also increases in T2DM (9) and selectively decreased by Ex-4 (Fig. 5, *G* and *H*) (27), suggesting that the essential effects of Ex-4 may be mediated by ICAM-1/Nox-4 axis. Exclusively in DIO group, we found concomitant increase in antioxidant molecules, namely SOD-1 and GPx (Fig. 6*D*). It remains ambiguous why Ex-4 had no effect on the antioxidant molecules in KK heart, which could be speculated because of the difference in genetic background, suggesting some caution regarding choosing model(s) when analyze the oxidative stress in T2DM.

M-CSF was found to be another Ex-4-sensitive cytokine in the present study (Fig. 5, *G* and *H*). M-CSF is a lineage-specific cytokine that promotes the survival, proliferation, and differentiation of mononuclear phagocytes (30), and, of note, its receptor increased collagen deposition within the myocardial infarct area (38), suggesting the M-CSF pathway might contribute to the generation in cardiac fibrosis that occurred in diabetic myocardium (Fig. 3, *C* and *D*), which could be another mechanism underlying the GLP-1R agonism-mediated reverse remodeling in diabetic myocardium. Future evaluation is desirable.

A study limitation of the present study is considered as follows: we had no data regarding the molecular mechanism how GLP-1 agonism may reverse cardiac steatosis. Excess lipid accumulation to non-adipocyte cells arises in the setting of dyslipidemia or lipid overload resulted from mismatch of lipid supply and consumption (31). This pathological lipid overload promotes lipotoxicity leading to pathological remodeling and dysfunction in local tissue. Indeed, the present study (Fig. 5, *A* and *B*) and previous data (20) demonstrated that GLP-1R activators mitigate dyslipidemia. When we consider the case of hepatic steatosis, this excellent study has been demonstrated that GLP-1 agonism markedly decreased hepatic content of cholesterols and phospholipids, accompanied by downregulation of hepatic lipogenesis-related genes and ApoB synthesis (26). Furthermore, it is also considerable that Ex-4 may modulate "cardiac" peroxisome proliferator-activated receptor-γ (PPAR-γ) because Ex-4 increases hepatic PPAR-γ expression in rat (34). PPAR-γ is primarily a regulator of lipid storage and transport in adipocytes and macrophages, and it elicits transdifferentiation of fibro- and myoblasts into adipocytes (11), suggesting the Ex-4 may reverse cardiac steatosis via modulating cardiac PPAR-γ axis. In addition to cardiomyocyte, Goto et al. (8) recently demonstrated that capillary endothelial PPAR-γ in heart promotes fatty acid uptake by heart in the postprandial state after long-term fasting. Taken together, the role of GLP-1R/PPAR-γ axis in cardiac steatosis seems unignorable, and future study is awaited.

In summary, the present study comprehensively demonstrated the advantage of therapeutic intervention for diabetic myocardial remodeling by exploring the GLP-1 axis-mediated molecular mechanisms.

ACKNOWLEDGMENTS

We thank Ikuyo Mizuguchi and Yoshikazu Fujita at the Division of Medical Research Engineering, Nagoya University Graduate School of Medicine, for technical support.

Present address of T. Shigeta: Div. of Cardiology, Gifu-prefectural Tajimi Hospital, 5-161, Maehata-cho, Tajimi, Gifu, 507-8522, Japan.

GRANTS

This work was supported in part by Ministry of Education, Culture, Sports, Science, and Technology Japan Grants-in-Aid for Scientific Research 20249045 and 23390208 (to T. Murohara) and 23591080 (to Y. K. Bando) and by the Suzuken Memorial Foundation (to Y. K. Bando).

DISCLOSURES

No conflicts of interest, financial or otherwise, are declared by the author(s).

AUTHOR CONTRIBUTIONS

A.M., T. Mitsui, M.A., and T.S. performed experiments; A.M., T. Mitsui, Y.K.B., and M.A. analyzed data; A.M. and Y.K.B. interpreted results of experiments; A.M., T. Mitsui, and Y.K.B. prepared figures; A.M. and Y.K.B. drafted manuscript; A.M., T. Mitsui, Y.K.B., M.A., T.S., and T. Murohara approved final version of manuscript; Y.K.B. conception and design of research; T. Murohara edited and revised manuscript.

REFERENCES

1. **Aguirre V, Werner ED, Giraud J, Lee YH, Shoelson SE, White MF.** Phosphorylation of Ser307 in insulin receptor substrate-1 blocks interactions with the insulin receptor and inhibits insulin action. *J Biol Chem* 277: 1531–1537, 2002.
2. **Ban K, Noyan-Ashraf MH, Hoefer J, Bolz SS, Drucker DJ, Husain M.** Cardioprotective and vasodilatory actions of glucagon-like peptide 1 receptor are mediated through both glucagon-like peptide 1 receptor-dependent and -independent pathways. *Circulation* 117: 2340–2350, 2008.
3. **Best JH, Hoogwerf BJ, Herman WH, Pelletier EM, Smith DB, Wenten M, Hussein MA.** Risk of cardiovascular disease events in patients with type 2 diabetes prescribed the glucagon-like peptide 1 (GLP-1) receptor agonist exenatide twice daily or other glucose-lowering therapies: a retrospective analysis of the LifeLink database. *Diabetes Care* 34: 90–95, 2011.
4. **Best JH, Lavillotti K, DeYoung MB, Garrison LP.** The effects of exenatide bid on metabolic control, medication use and hospitalization in patients with type 2 diabetes mellitus in clinical practice: a systematic review. *Diabetes Obes Metab* 14: 387–398, 2012.
5. **Boudina S, Abel ED.** Diabetic cardiomyopathy revisited. *Circulation* 115: 3213–3223, 2007.
6. **Boudina S, Bugger H, Sena S, O'Neill BT, Zaha VG, Ilkun O, Wright JJ, Mazumder PK, Palfreyman E, Tidwell TJ, Theobald H, Khalimonchuk O, Wayment B, Sheng X, Rodnick KJ, Centini R, Chen D, Litwin SE, Weimer BE, Abel ED.** Contribution of impaired myocardial insulin signaling to mitochondrial dysfunction and oxidative stress in the heart. *Circulation* 119: 1272–1283, 2009.
7. **Chaudhuri A, Ghanim H, Vora M, Sia CL, Korzeniewski K, Dhindsa S, Makdissi A, Dandona P.** Exenatide exerts a potent antiinflammatory effect. *J Clin Endocrinol Metab* 97: 198–207, 2012.
8. **Goto K, Iso T, Hanaoka H, Yamaguchi A, Suga T, Hattori A, Irie Y, Shinagawa Y, Matsui H, Syamsunarno MR, Matsui M, Haque A, Arai M, Kunimoto F, Yokoyama T, Endo K, Gonzalez FJ, Kurabayashi M.** Peroxisome proliferator-activated receptor-gamma in capillary endothelia promotes fatty acid uptake by heart during long-term fasting. *J Am Heart Assoc* 2: e004861, 2013.
9. **Gu HF, Ma J, Gu KT, Brismar K.** Association of intercellular adhesion molecule 1 (ICAM1) with diabetes and diabetic nephropathy. *Front Endocrinol (Lausanne)* 3: 179, 2012.
10. **Holst JJ, Gromada J.** Role of incretin hormones in the regulation of insulin secretion in diabetic and nondiabetic humans. *Am J Physiol Endocrinol Metab* 287: E199–E206, 2004.

11. **Hu E, Tontonoz P, Spiegelman BM.** Transdifferentiation of myoblasts by the adipogenic transcription factors PPAR gamma and C/EBP alpha. *Proc Natl Acad Sci USA* 92: 9856–9860, 1995.
12. **Huang C, Andres AM, Ratliff EP, Hernandez G, Lee P, Gottlieb RA.** Preconditioning involves selective mitophagy mediated by Parkin and p62/SQSTM1. *PLoS One* 6: e20975, 2011.
13. **Kim F, Pham M, Luttrell I, Bannerman DD, Tupper J, Thaler J, Hawn TR, Raines EW, Schwartz MW.** Toll-like receptor-4 mediates vascular inflammation and insulin resistance in diet-induced obesity. *Circ Res* 100: 1589–1596, 2007.
14. **Kondo K, Nozawa K, Tomita T, Ezaki K.** Inbred strains resulting from Japanese mice. *Bull Exp Anim* 6: 107–112, 1957.
15. **Lee YS, Park MS, Choung JS, Kim SS, Oh HH, Choi CS, Ha SY, Kang Y, Kim Y, Jun HS.** Glucagon-like peptide-1 inhibits adipose tissue macrophage infiltration and inflammation in an obese mouse model of diabetes. *Diabetologia* 55: 2456–2468, 2012.
16. **Maejima Y, Kuroda J, Matsushima S, Ago T, Sadoshima J.** Regulation of myocardial growth and death by NADPH oxidase. *J Mol Cell Cardiol* 50: 408–416, 2011.
17. **Mahadev K, Motoshima H, Wu X, Ruddy JM, Arnold RS, Cheng G, Lambeth JD, Goldstein BJ.** The NAD(P)H oxidase homolog Nox4 modulates insulin-stimulated generation of H_2O_2 and plays an integral role in insulin signal transduction. *Mol Cell Biol* 24: 1844–1854, 2004.
18. **Matsushima S, Kuroda J, Ago T, Zhai P, Park JY, Xie LH, Tian B, Sadoshima J.** Increased oxidative stress in the nucleus caused by Nox4 mediates oxidation of HDAC4 and cardiac hypertrophy. *Circ Res* 112: 651–663, 2013.
19. **Mells JE, Fu PP, Sharma S, Olson D, Cheng L, Handy JA, Saxena NK, Sorescu D, Anania FA.** Glp-1 analog, liraglutide, ameliorates hepatic steatosis and cardiac hypertrophy in C57BL/6J mice fed a Western diet. *Am J Physiol Gastrointest Liver Physiol* 302: G225–G235, 2012.
20. **Mundil D, Cameron-Vendrig A, Husain M.** GLP-1 receptor agonists: a clinical perspective on cardiovascular effects. *Diab Vasc Dis Res* 9: 95–108, 2012.
21. **Naik E, Dixit VM.** Mitochondrial reactive oxygen species drive proinflammatory cytokine production. *J Exp Med* 208: 417–420, 2011.
22. **Nikolaidis LA, Elahi D, Hentosz T, Doverspike A, Huerbin R, Zourelias L, Stolarski C, Shen YT, Shannon RP.** Recombinant glucagon-like peptide-1 increases myocardial glucose uptake and improves left ventricular performance in conscious dogs with pacing-induced dilated cardiomyopathy. *Circulation* 110: 955–961, 2004.
23. **Noyan-Ashraf MH, Momen MA, Ban K, Sadi AM, Zhou YQ, Riazi AM, Baggio LL, Henkelman RM, Husain M, Drucker DJ.** GLP-1R agonist liraglutide activates cytoprotective pathways and improves outcomes after experimental myocardial infarction in mice. *Diabetes* 58: 975–983, 2009.
24. **Noyan-Ashraf MH, Shikatani EA, Schuiki I, Mukovozov I, Wu J, Li RK, Volchuk A, Robinson LA, Billia F, Drucker DJ, Husain M.** A glucagon-like peptide-1 analog reverses the molecular pathology and cardiac dysfunction of a mouse model of obesity. *Circulation* 127: 74–85, 2013.
25. **Papanicolaou KN, Ngoh GA, Dabkowski ER, O'Connell KA, Ribeiro RF Jr, Stanley WC, Walsh K.** Cardiomyocyte deletion of mitofusin-1 leads to mitochondrial fragmentation and improves tolerance to ROS-induced mitochondrial dysfunction and cell death. *Am J Physiol Heart Circ Physiol* 302: H167–H179, 2012.
26. **Parlevliet ET, Wang Y, Geerling JJ, Schroder-Van der Elst JP, Picha K, O'Neil K, Stojanovic-Susulic V, Ort T, Havekes LM, Romijn JA, Pijl H, Rensen PC.** GLP-1 receptor activation inhibits VLDL production and reverses hepatic steatosis by decreasing hepatic lipogenesis in high-fat-fed APOE*3-leiden mice. *PLoS One* 7: e49152, 2012.
27. **Pattillo CB, Pardue S, Shen X, Fang K, Langston W, Jourd'heuil D, Kavanagh TJ, Patel RP, Kevil CG.** ICAM-1 cytoplasmic tail regulates endothelial glutathione synthesis through a NOX4/PI3-kinase-dependent pathway. *Free Radic Biol Med* 49: 1119–1128, 2010.
28. **Raddatz E, Thomas AC, Sarre A, Benathan M.** Differential contribution of mitochondria, NADPH oxidases, and glycolysis to region-specific oxidant stress in the anoxic-reoxygenated embryonic heart. *Am J Physiol Heart Circ Physiol* 300: H820–H835, 2011.
29. **Rijzewijk LJ, van der Meer RW, Smit JW, Diamant M, Bax JJ, Hammer S, Romijn JA, de Roos A, Lamb HJ.** Myocardial steatosis is an independent predictor of diastolic dysfunction in type 2 diabetes mellitus. *J Am Coll Cardiol* 52: 1793–1799, 2008.
30. **Roth P, Stanley ER.** The biology of CSF-1 and its receptor. *Curr Top Microbiol Immunol* 181: 141–167, 1992.
31. **Schaffer JE.** Lipotoxicity: when tissues overeat. *Curr Opin Lipidol* 14: 281–287, 2003.
32. **Schenk S, Saberi M, Olefsky JM.** Insulin sensitivity: modulation by nutrients and inflammation. *J Clin Invest* 118: 2992–3002, 2008.
33. **Shigeta T, Aoyama M, Bando YK, Monji A, Mitsui T, Takatsu M, Cheng XW, Okumura T, Hirashiki A, Nagata K, Murohara T.** Dipeptidyl peptidase-4 modulates left ventricular dysfunction in chronic heart failure via angiogenesis-dependent and -independent actions. *Circulation* 126: 1838–1851, 2012.
34. **Svegliati-Baroni G, Saccomanno S, Rychlicki C, Agostinelli L, De Minicis S, Candelaresi C, Faraci G, Pacetti D, Vivarelli M, Nicolini D, Garelli P, Casini A, Manco M, Mingrone G, Risaliti A, Frega GN, Benedetti A, Gastaldelli A.** Glucagon-like peptide-1 receptor activation stimulates hepatic lipid oxidation and restores hepatic signalling alteration induced by a high-fat diet in nonalcoholic steatohepatitis. *Liver Int* 31: 1285–1297, 2011.
35. **Taketomi S, Ikeda H, Ishikawa E, Iwatsuka H.** Determination of overall insulin sensitivity in diabetic mice, KK. *Horm Metab Res* 14: 14–18, 1982.
36. **van de Weijer T, Schrauwen-Hinderling VB, Schrauwen P.** Lipotoxicity in type 2 diabetic cardiomyopathy. *Cardiovasc Res* 92: 10–18, 2011.
37. **Wang Y, Nartiss Y, Steipe B, McQuibban GA, Kim PK.** ROS-induced mitochondrial depolarization initiates PARK2/PARKIN-dependent mitochondrial degradation by autophagy. *Autophagy* 8: 1462–1476, 2012.
38. **Yano T, Miura T, Whittaker P, Miki T, Sakamoto J, Nakamura Y, Ichikawa Y, Ikeda Y, Kobayashi H, Ohori K, Shimamoto K.** Macrophage colony-stimulating factor treatment after myocardial infarction attenuates left ventricular dysfunction by accelerating infarct repair. *J Am Coll Cardiol* 47: 626–634, 2006.
39. **Yoon YS, Uchida S, Masuo O, Cejna M, Park JS, Gwon HC, Kirchmair R, Bahlman F, Walter D, Curry C, Hanley A, Isner JM, Losordo DW.** Progressive attenuation of myocardial vascular endothelial growth factor expression is a seminal event in diabetic cardiomyopathy: restoration of microvascular homeostasis and recovery of cardiac function in diabetic cardiomyopathy after replenishment of local vascular endothelial growth factor. *Circulation* 111: 2073–2085, 2005.
40. **Zeyda M, Stulnig TM.** Obesity, inflammation, and insulin resistance—a mini-review. *Gerontology* 55: 379–386, 2009.